Induction Machine Control Systems with Magnetic Saturation

Chaofu Kao Charles R. Sullivan Brian Acker Seth R. Sanders
Department of Electrical Engineering and Computer Sciences
University of California, Berkeley

Abstract— A new induction machine model that includes the effects of magnetic saturation is developed through magnetic circuit modeling. The new model has advantages for use in designing control systems, and is applied to the design of field-oriented control schemes for saturated machines. The control methods are extensions of standard field-oriented methods for linear-magnetics machines, but remove cross coupling between rotor flux control and torque control that are produced by magnetic saturation. An observer for estimating rotor flux is also discussed. Experimental results verifying operation of the proposed control method are presented.

I. Introduction

Induction machines are usually modeled with the assumption of linear magnetics. However, in many variable-torque applications, it is desirable to operate in saturation, allowing an induction machine to produce higher torque. For example, in vehicular applications, the induction machine may be sized for normal road conditions. However, to overcome extreme inclines or to permit high acceleration and deceleration rates, it is necessary to produce high instantaneous torque. Thus, a smaller machine may be used if its control system can maintain control through peak torque demand. Traditionally, inductance values used for control or calculations are adjusted to compensate for saturation effects. However, this is not always adequate. More precise modeling of saturation becomes essential for control purposes and for understanding the limitations imposed by saturation. This paper develops a new model for saturation and discusses its implications for control systems.

It has been recently noted that saturation effects in smooth air-gap machines can introduce cross-coupling effects that are not predicted by linear models. In a two-axis machine (or model) the current in one winding can affect the flux in the orthogonal winding. The 'cross saturation' model [1-8] has become the standard method of accounting for these effects. The model is based on the conventional T model of an induction motor, and the saturation is assumed to be entirely in the mutual inductance, not in the leakage. While the T model with saturating mutual inductance gives reasonable accuracy in simulations, it can be inconvenient to use when the machine is connected to a voltage source, since it is most naturally a current-controlled rather than a flux-controlled model. In [4], for example, the T model is transformed to a π model for purposes of simulation.

The authors would like to acknowledge support from an NSF graduate fellowship, a GE graduate fellowship, and NSF grant ECS-9358284.

0-7803-1859-5/94/$4.00 © 1994 IEEE

Because the form of the T model with saturating mutual inductance is merely postulated by extending a standard linear model to include saturation of the mutual path, our work develops a new model, based on a nonlinear magnetic circuit model of the machine [9]. The resulting machine model is in fact most naturally a π model, and so we avoid the need to transform it for simulations and/or control designs. Although the π model can provide a more accurate model for the saturated induction machine, of greater importance, the π form is more convenient for field-oriented control designs that take magnetic saturation into account.

Field-oriented control decouples the control of rotor flux and torque in the linear-magnetics case. However, cross-saturation effects can severely disrupt performance of a control system designed without taking these effects into account [10]. Although control systems based on the T model and the use of a current source inverter have been developed to mitigate these problems [6, 11, 12, 13], the resulting designs are somewhat awkward. In contrast, with the flux-controlled π model, by using the stator flux as an intermediate control variable, it is possible to obtain a simple decoupled control of rotor flux and torque. Our approach relies on the use of a fast control loop around a voltage source inverter to control stator flux. Stator flux is then used as an intermediate control variable, as is stator current in current-fed control schemes.

As with standard field-oriented control, a method of estimating rotor flux without direct measurement is desirable, and we will discuss a method for doing this with the new model. Measurements taken on a 3 hp wound rotor induction machine show good correlation with our model. We refer the reader to [9] for details. The present paper includes a description of an experimental set-up of the proposed control system, along with detailed test results.

II. Magnetic Circuit Modeling

To model a saturating magnetic structure we use conventional magnetic circuit modeling, augmented by the use of nonlinear reluctances to represent sections of saturable steel or other soft ferromagnetic material. The B-H characteristic of the steel is assumed to be described by a single-valued nonlinear monotonic function. The flux/MMF characteristic of the reluctance element, for simple geometries, is just the B-H characteristic, scaled by cross-sectional area for flux, and by length for MMF.

Figure 1 a) shows a simplified tooth structure for a single pair of teeth in an induction machine. Figure 1 b)

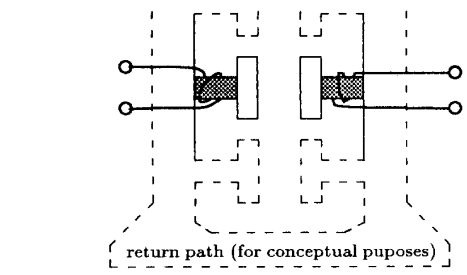

a)

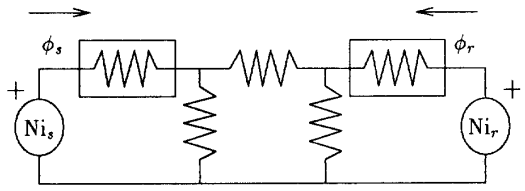

b)

Fig. 1. Model of Tooth Pair. a) Simplified physical structure. b) Corresponding magnetic circuit. Boxed elements are nonlinear.

shows one way of drawing a magnetic circuit model for the tooth pair, making the assumption that the only portions of the steel that saturate are the central legs, shown shaded in Figure 1 a).

Through a series of transformations [9], the magnetic circuit can be shown to be equivalent to the electric circuit in Figure 2. We separate the stator and rotor induc-

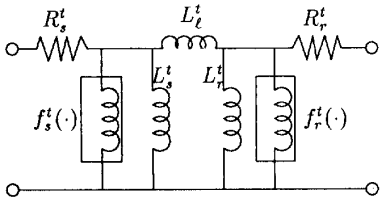

Fig. 2. Electric Circuit of Tooth Pair

tances into linear parts, L_s^t and L_r^t, and nonlinear parts, with flux-current relationships $f_s^t(\cdot)$ and $f_r^t(\cdot)$. The superscript t is used to indicate an inductance or function describing only a single tooth. As drawn, the circuit in Figure 2 could have circulating currents in various loops of inductors. In the linear case these are unobservable, uncontrollable modes. In the nonlinear case, the circulating current would not appear directly at the rotor and stator terminals, yet could affect the apparent nonlinear characteristics of the inductances. However, additional constraints resulting from the magnetic circuit preclude this possibility. Namely, the flux linkage in L_ℓ^t must be equal to the difference in flux linkages in L_r^t and L_s^t, the flux linkages in $f_s^t(\cdot)$ and L_s^t must be equal, and the flux linkages in $f_r^t(\cdot)$ and L_r^t must be equal.

To move from the model of a single tooth pair to a model of a symmetric induction machine, we assume a smooth air-gap and perfectly sinusoidally distributed windings. To model this structure, we consider the rotor and stator to be constructed of an infinite number of infinitesimal teeth of the type modeled above, each with the appropriate number of turns of each phase, according to the sinusoidal distribution. The circuit model of the complete machine has the same structure as the model in Figure 2, but each element has vector voltages and currents. We use a two-axis model, and note that the standard transformations may be used to model a three-phase machine. The nonlinear inductors are described by vector functions of the form $\vec{\imath} = F(\vec{\lambda})$. The vector direction of $\vec{\imath}$ is the same as the direction of $\vec{\lambda}$, and rotational symmetry implies that $||\vec{\imath}||$ depends only on $||\vec{\lambda}||$. As a result of these two constraints, $F(\cdot)$ may be written as

$$F(\vec{\lambda}) = f(||\vec{\lambda}||)\frac{\vec{\lambda}}{||\vec{\lambda}||}. \tag{1}$$

The function $f(\cdot)$ is a scalar function that is shaped similarly to the saturation characteristic of the individual teeth, $f^t(\cdot)$, but is produced by the combination of the saturation characteristics of the steel in many teeth acting simultaneously [9]. It may be assumed to be monotonic, and, if hysteresis is neglected, to be single valued and to pass through the origin. Note that one could consider the quantity $||\vec{\lambda}||/f(||\vec{\lambda}||)$ to be an inductance that varies as a function of $||\vec{\lambda}||$, so that $\vec{\imath} = \vec{\lambda}/L(||\vec{\lambda}||)$. This is the notation used in most discussions of the nonlinear T model, and is mathematically equivalent. We choose to use the $F(\cdot)$ notation instead, because it clarifies which terms in an equation are linear and which are not. We also choose $F(\cdot)$ to include only the nonlinear portion of the inductance, and absorb any linear part in a parallel linear inductance. With this notation, the linear-magnetics case can be obtained from any of our expressions simply by dropping the nonlinear terms.

The electrical dynamics of the system using the functions $F_s(\cdot)$ and $F_r(\cdot)$, and with rotation of the rotor are

$$\vec{\imath}_s^s = F_s(\vec{\lambda}_s^s) + (\frac{1}{L_s} + \frac{1}{L_\ell})\vec{\lambda}_s^s - \frac{1}{L_\ell}e^{\mathbf{J}\theta}\vec{\lambda}_r^r \tag{2}$$

$$\vec{\imath}_r^r = F_r(\vec{\lambda}_r^r) + (\frac{1}{L_r} + \frac{1}{L_\ell})\vec{\lambda}_r^r - \frac{1}{L_\ell}e^{-\mathbf{J}\theta}\vec{\lambda}_s^s, \tag{3}$$

and

$$\dot{\vec{\lambda}}_s^s = \vec{v}_s^s - \mathbf{R}_s\,\vec{\imath}_s^s \tag{4}$$

$$\dot{\vec{\lambda}}_r^r = \vec{v}_r^r - \mathbf{R}_r\,\vec{\imath}_r^r, \tag{5}$$

where θ is the electrical angle of the rotor position, $\mathbf{J}$ is the rotation matrix

$$\mathbf{J} = \begin{bmatrix} 0 & -1 \\ 1 & 0 \end{bmatrix},$$

and the overdot ($\dot{}$) indicates differentiation with respect to time. Note that L_s and L_r denote the linear parts of the magnetizing inductances associated with the stator and rotor, respectively. They are not, as in conventional T model notation, the overall inductance measured from the stator and rotor terminals. Due to the symmetry of the machine, the resistance matrices $\mathbf{R}_s$ and $\mathbf{R}_r$ are just the identity multiplied by scalar resistances. The subscript s or r on flux linkage or current (λ or i) indicates stator or rotor quantities. The superscript s indicates that the flux or current is measured in the stator, or stationary, reference frame, and the superscript r indicates coordinates fixed to the mechanical rotation of the rotor. We use different superscripts to designate the transformed quantities in different reference frames, summarized below:

superscript designation	reference frame	ρ
s	Stator	$\rho = 0$
r	Rotor	$\rho = \theta$
x	Arbitrary	ρ
e	Field-Oriented	$\angle(\vec{\lambda}_r^s)$

Experimental measurements have been conducted on a 3 hp wound-rotor machine. Both a T model with saturation in the mutual path, and the above described π model have been fit to the measured data. The π model shows a slightly better fit [9], and is much better suited to control design as discussed in Section III.

III. Field-Oriented Control

In field-oriented control, the use of a reference frame oriented in the direction of the rotor flux vector results in decoupled control of rotor flux and torque [6, 14]. For use with the nonlinear flux-controlled model, we formulate the field-oriented control method in terms of flux vectors as state variables. We first discuss the control as if we had available measurements of all state variables. Later sections will discuss methods of measuring or estimating relevant variables. To transform to the rotor field-oriented reference frame, we use the Park transformation [9], with ρ set equal to the angle of the rotor flux vector $\vec{\lambda}_r^s$. We use the superscript e, for electrical, to designate variables in the rotor field-oriented reference frame, since, in steady state, this reference frame rotates at the same frequency as the supply voltage. Notice that setting $\rho = \angle(\vec{\lambda}_r^s)$ is equivalent to constraining λ_{rq}^e to be zero, and results in

$$\dot{\rho} = \frac{R_r}{L_\ell}\frac{\lambda_{sq}^e}{\lambda_{rd}^e} + \dot{\theta}\,. \tag{6}$$

The other electrical equations become

$$\dot{\lambda}_{rd}^e = -R_r\left[(\tfrac{1}{L_r}+\tfrac{1}{L_\ell})\lambda_{rd}^e - \tfrac{1}{L_\ell}\lambda_{sd}^e + f_r(\lambda_{rd}^e)\right] \tag{7}$$

$$\begin{aligned}\dot{\vec{\lambda}}_s^e = & -\dot{\rho}\,\mathbf{J}\vec{\lambda}_s^e + \vec{v}_s^e \\ & -R_s\left\{(\tfrac{1}{L_s}+\tfrac{1}{L_\ell})\vec{\lambda}_s^e - \tfrac{1}{L_\ell}\begin{bmatrix}\lambda_{rd}^e\\ 0\end{bmatrix} + F_s(\vec{\lambda}_s^e)\right\}\end{aligned} \tag{8}$$

where $f_r(\cdot)$ is the scalar version of $F_r(\cdot)$, as in (1), and the rotor voltage is zero for shorted rotor windings or shorted rotor bars. The mechanical equations become

$$\dot{\omega} = \frac{1}{J_{inertia}}(\tau(\vec{\lambda}_s^x, \vec{\lambda}_r^x, \theta) - \tau_{load}) \tag{9}$$

$$\dot{\theta} = \omega. \tag{10}$$

where the torque $\tau(\vec{\lambda}_s^x, \vec{\lambda}_r^x, \theta)$, in terms of the Park-transformed flux is [9],

$$\tau(\vec{\lambda}_s^x, \vec{\lambda}_r^x, \theta) = \left[\frac{1}{L_\ell}\mathbf{J}\vec{\lambda}_r^x\right]^T\vec{\lambda}_s^x = -\frac{1}{L_\ell}(\lambda_{sd}^x\lambda_{rq}^x - \lambda_{sq}^x\lambda_{rd}^x) \tag{11}$$

This expression is identical to one form of the expression for the torque with linear magnetics. It can be shown to be equivalent to another common form,

$$\tau = \vec{i}_s^{\,x\,T}\mathbf{J}\vec{\lambda}_s^x. \tag{12}$$

These equations, though formulated in terms of flux, reduce to the familiar equations for field-oriented control when they are reformulated in terms of stator current, and the nonlinear terms are dropped. Unfortunately, nonlinear terms in the conversion to a stator current formulation add cross coupling, destroying the simplicity of the control. Similar cross coupling in a T model has been shown in simulations to cause significant disruptions when control algorithms that ignore it are used [10]. However, cross coupling does not appear in the flux formulation in (6)-(10) above, except in the stator flux dynamics (8). This cross coupling, due to the stator resistive drop term, can be avoided, and will be discussed later in this section. Here lies one of the advantages of the π model with respect to the T model. By viewing stator flux as a control variable, as opposed to stator current, we obtain a simple decoupled control for rotor flux magnitude and for torque. Specifically, the component of the stator flux aligned with the rotor flux can be used to control rotor flux magnitude, per (7), while the orthogonal component of stator flux can be used to control torque, per (9).

Note that in equation (7), the rotor flux does have a nonlinearity not present in the linear-magnetics case. But this subsystem is not hard to control. It can be stabilized with simple linear feedback, or may be linearized with feedback by using

$$\lambda_{sd}^e = L_\ell\left\{(\frac{1}{L_r}+\frac{1}{L_\ell})\lambda_{rd}^e + f_r(\lambda_{rd}^e)\right\} - K_d\frac{L_\ell}{R_r}(\lambda_{rd}^e - \tilde{\lambda}_{rd}^e), \tag{13}$$

where K_d is the desired linear feedback coefficient.

Since control of stator flux provides decoupled control of torque and rotor flux, the stator flux command is used as an input to a subsystem that controls the stator flux. The controller subtracts the terms for resistive drop and speed voltage in equation (8), so that the system looks simply like an integrator. Then, the rest of the control can be as simple as linear feedback,

$$\begin{aligned}\tilde{\vec{v}}_s^e = & K(\tilde{\vec{\lambda}}_s^e - \vec{\lambda}_s^e) + \dot{\rho}\,\mathbf{J}\vec{\lambda}_s^e \\ & +R_s\left\{(\tfrac{1}{L_s}+\tfrac{1}{L_\ell})\vec{\lambda}_s^e - \tfrac{1}{L_\ell}\begin{bmatrix}\lambda_{rd}^e\\ 0\end{bmatrix} + F_s(\vec{\lambda}_s^e)\right\}.\end{aligned} \tag{14}$$

Notice that the only difference that saturation makes in the design of this inner stator flux-control loop is the addition of $F_s(\cdot)$ in the term representing resistive drop in (14). If stator current is measured, the measured current may be used in the control, and so the characteristics of the nonlinearity are not needed for the controller as discussed in equation (2). The control is then

$$\tilde{\vec{v}}_s^e = K(\tilde{\vec{\lambda}}_s^e - \vec{\lambda}_s^e) + \dot{\rho}\,\mathbf{J}\vec{\lambda}_s^e + R_s\vec{i}_s^e. \qquad (15)$$

Thus, in this implementation the control is completely independent of the magnetic saturation, except for the rotor nonlinearity's effect on the rotor flux magnitude control loop, where it may be ignored. This is in contrast to a similar system, based on the nonlinear T model in [12]. The system in [12] is shown to require additional terms to cancel cross coupling due to the nonlinearity. Although the control based on the π model is independent of the magnetic nonlinearity, this is not true of the observers, so a complete implementation will require knowledge of the nonlinearity.

IV. Flux Observers

Since the stator voltages and currents of a squirrel cage motor can be measured directly, a stator-based observer is attractive. Some stator-based observers, such as those discussed in [15], integrate the derivative of rotor flux, calculated from measurements of stator quantities. With the nonlinear model, nonlinear dynamics in the observer and in the observer error would result. To avoid this, we estimate the stator flux instead, and then make an instantaneous calculation, involving no dynamics, of the rotor flux. The observer is defined by

$$\dot{\hat{\vec{\lambda}}}_s^s = \vec{v}_s^s - R_s\vec{i}_s^s - K\hat{\vec{\lambda}}_s^s \qquad (16)$$

where $\hat{}$ indicates an estimate. A decay term such as $K\hat{\vec{\lambda}}_s^s$ must be used in order to make the observer asymptotically stable. The calculation of the rotor flux is accomplished by

$$\hat{\vec{\lambda}}_r^s = L_\ell\left[\left(\frac{1}{L_s} + \frac{1}{L_\ell}\right)\hat{\vec{\lambda}}_s^s + F_s(\hat{\vec{\lambda}}_s^s) - \vec{i}_s^s\right]. \qquad (17)$$

Note that no speed or position estimates are required for this observer, or for the field-oriented control itself. In many systems the generation of a torque command may require these measurements, but the torque control itself does not. Another advantage of this observer is that the rotor saturation characteristic does not appear in the equations, and so does not need to be known. Since it is not critical to know the rotor saturation characteristic for the control either, this feature of this observer would make possible a complete control system that did not require knowledge of the rotor saturation characteristic.

An disadvantage of this observer is the necessity for the inclusion of a decay term, because the term introduces error at low frequencies. Results with linear-magnetics systems show a practical lower limit for this type of system is about 3 Hz. With separate coils used for sensing flux, systems have been reported to work well above 0.5 Hz [14]. While these results would be satisfactory for many speed-control applications, a different observer is required for position control [16].

V. Experimental Set-Up

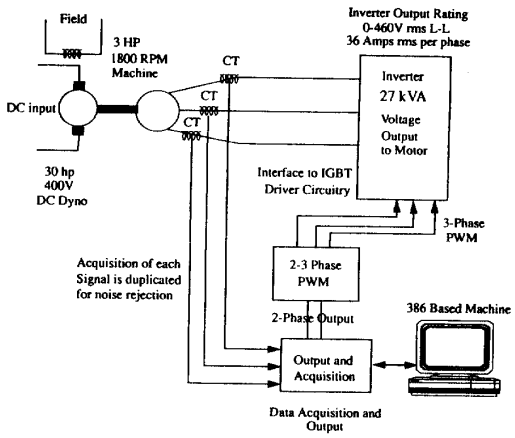

Fig. 3. Experimental Set-Up

Our experimental set-up is illustrated in Figure 3. The induction machine used in the experiments is a 3hp, 1800rpm wound rotor machine, rated for 220V rms line-to-line, and operated with the rotor shorted. The motor is fed from a commercial pulse-width modulated (PWM) IGBT inverter, operating at a switching frequency of 15kHz, and rated for 36A and 460V rms line-to-line. As such, it is possible to drive the motor well above its ratings. The microprocessor controller within the inverter was replaced with custom hardware that directly accesses the gate driver modules. The custom hardware consists of a three phase PWM modulator that interfaces with two-axis command voltages supplied by our digital controller, a 386-based personal computer.

The data collection and output to the inverter is provided by a commercial data acquisition/data output board. The data acquisition function features an eight channel differential multiplexer, with data conversion rate of 100kHz. The input signals consisting of the motor phase currents are filtered prior to sampling. Since this system has excess sampling capacity, duplicate samples of each signal are obtained at each sampling time. Selection between the duplicate signal samples is accomplished by examining their proximity to estimates predicted within the control system. This greatly improves rejection of bad data corrupted by noise spikes.

A 386-based personal computer is used to implement the control algorithm. Computer interrupts are generated at 1 KHz to permit a 1 ms update rate. Performance tests have shown that the control system is capable of updates at 0.5 ms. The excess time between interrupts is utilized to control the computer display. User selectable plots in the electrical reference frame and/or the stator reference frame can be displayed in real-time. Command torque and flux levels can be preprogrammed or changed in real-time from the keyboard. Both open and closed loop control as well as adjustments are available through

keyboard interface.

A 30 horsepower separately excited dynamometer is used to provide adjustable loading, and is fitted with a torque scale used to measure mechanical torque.

A. Implementation of Control and Flux Estimation Schemes

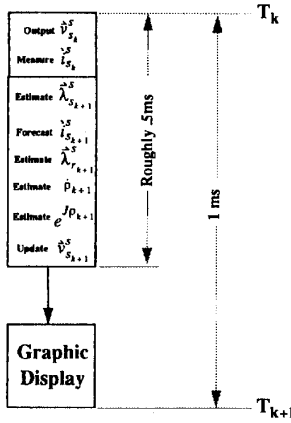

Fig. 4. Timeline for Execution of Control

Our initial experimental implementation is based on the stator flux control scheme outlined in Section 3 coupled with the stator-flux-based rotor flux observer outlined in Section 4. Since our experimental framework restricts the update rate to be on the order of 1 ms, care needs to be taken in implementing these control and estimation schemes. For example, a delay of 1 ms at an electrical frequency of 60Hz amounts to a phase delay of 21 degrees, which could cause a severe disruption to any field oriented control scheme. To be precise and consistent, our algorithm is executed according to the time line shown in Figure 4. In particular, after an interrupt at t_k, the voltage $\vec{v}^s_{s\ k}$ is fed to the inverter PWM controller through a zero-order hold. Immediately thereafter, the motor phase currents $\vec{i}^s_{s\ k}$ are sampled. Over the remainder of the 1 ms interval, the state of the flux observer is updated, the next value of the control $\vec{v}^s_{s\ k+1}$ is computed, and the computer display is updated.

A functional block diagram of the complete control algorithm is shown in Figure 5. Conceptually, this algorithm is divided into five subblocks, which are discussed in the sequel.

1) Rotor Flux Estimation: This block implements a discrete time version of the stator-flux-based scheme outlined in Section 5. Specifically, during the k-th sample interval, this block uses the commanded voltage $\vec{v}_{s\ k}$, the sampled current $\vec{i}_{s\ k}$, and the stator flux estimate $\hat{\vec{\lambda}}_{s\ k}$ to update the stator flux estimate according to

$$\hat{\vec{\lambda}}_{s\ k+1} = \hat{\vec{\lambda}}_{s\ k} + T(\vec{v}_{s\ k} - R_s\vec{i}_{s\ k} - K_o\hat{\vec{\lambda}}_{s\ k}) \qquad (18)$$

where T is the (1 mS) sampling interval and K_o is a factor used to stabilize the observer, as previously discussed. An estimate for the rotor flux vector $\hat{\vec{\lambda}}_{r\ k+1}$ at the $(k+1)$-th sample time is then constructed using the static equation (17) from the now-available stator flux estimate and a one-step-advanced version of the measured stator current vector. The latter is developed as follows.

2) One-Step Prediction of Stator Current: Our control/estimation algorithm uses a one-step-advanced version of the sampled current in some functions. To develop this predicted current vector, the sampled current vector is rotated ahead through one time step in accord with an available estimate of the electrical angular frequency. The estimate of the angular frequency is developed by numerically differentiating the estimate of the rotor flux vector with respect to time. The predicted stator current vector is constructed by

$$\hat{\vec{i}}_{s\ k+1} = e^{\mathbf{J}(\hat{\rho}_k T)}\vec{i}_{s\ k} \qquad (19)$$

with the estimate of the electrical angular velocity $\hat{\rho}_k$ developed as follows.

3) Estimate of Electrical Angular Velocity: Our flux estimation algorithm attempts to keep track of the instantaneous value of the rotor flux vector. As such, an estimate of the instantaneous angular position of this vector is always available. Specifically, our algorithm stores this angular information in the matrix

$$e^{\mathbf{J}\hat{\rho}_k} = \frac{1}{\|\hat{\vec{\lambda}}_{r\ k}\|}\begin{bmatrix} \hat{\lambda}_{rd\ k} & -\hat{\lambda}_{rq\ k} \\ \hat{\lambda}_{rq\ k} & \hat{\lambda}_{rd\ k} \end{bmatrix}$$

which has entries consisting of the cosine and sine of the rotor flux angle. In this way, any difficulties arising in keeping track of angle modulo 2π are avoided.

The instantaneous electrical frequency (of the rotor flux vector) is calculated by differentiating the relationship $\vec{\lambda}^e_r = e^{-\mathbf{J}\rho}\vec{\lambda}^s_r$, and then examining the second component of the resulting vector equation. The result is

$$\dot{\rho} = \frac{[0\ 1]e^{-\mathbf{J}\rho}\dot{\vec{\lambda}}^s_r}{\lambda^e_{rd}}. \qquad (20)$$

Our algorithm develops an estimate of the electrical frequency with a bandlimited numerical differentiation scheme applied to the sequence of rotor flux estimates. Note that direct calculation and differentiation of the flux angle is always avoided.

4) Calculation of Command Voltage: The desired inverter voltage for step $k+1$ is calculated using the commanded torque and the commanded rotor flux magnitude, which are used to develop a commanded stator flux. In our initial experiments, the rotor flux magnitude has been controlled with an open-loop scheme where an appropriate direct axis stator flux is specified a priori. This corresponds to the choice $K_d = 0$ in (13).

The commanded stator flux is compared to the estimated value of this flux, $\hat{\vec{\lambda}}_{s\ k+1}$, to develop an error signal. The error signal is multiplied by a feedback gain and then added to a feedforward term comprised from the predicted stator current and a predicted speed voltage. This implements the control (15).

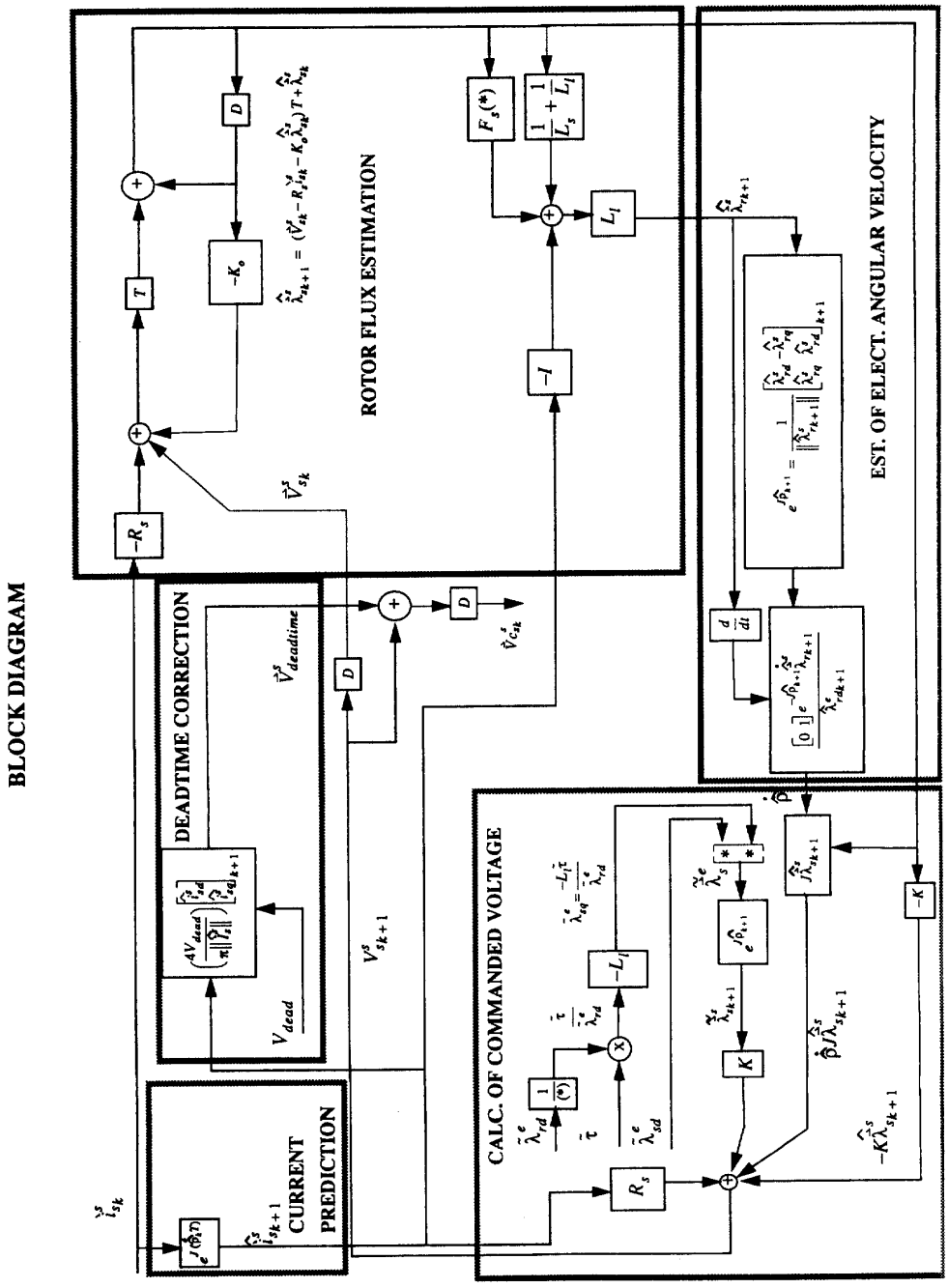

Fig. 5. Control System Block Diagram

5) Deadtime Correction: The final block in our algorithm is a deadtime correction scheme that attempts to counteract the voltage errors caused by deadtime in the inverter. Note that the deadtime voltage error depends only on the sign of the current in each phase of the inverter, and causes a voltage error of the form $\Delta v = -V_{dead} sgn(i)$. It turns out that attempting to directly compensate for this term is difficult since one would then need to detect the zero crossings of the current. This is difficult due to noise corrupting the current measurements, which can lead to a bouncing measured current signal. An alternative is to compensate only for the fundamental component of the deadtime voltage by multiplying the (approximately sinusoidal) current by the factor $4V_{dead}/(\pi\|\vec{i}_s\|)$ where $V_{dead} = V_{DCbus} f_s t_{dead}$ is the product of the dc bus voltage, the switching frequency, and the inverter dead time. In our system, this amounted to about 40 volts. This technique is motivated by the describing function method and has been reported to be effective in [17]. In particular, this approach avoids excessive sensitivity to current zero crossings.

VI. Experimental Results

Experiments studying instantaneous control of torque were carried out with the system described above. Specifically, our system commands a step torque waveform to allow observations of certain measured and estimated quantities. Experiments were carried out in two ways. Firstly, we used the control law based on the nonlinear flux-current model for the magnetizing inductances in our π model. The second experiments used only linear inductance models in the design of the control law. This amounted to a trivial modification where a look-up table containing the nonlinear flux-current relation for the stator is replaced with a look-up table containing a linear flux-current relation. The two flux-current curves are compared in Figure 6. Note that the linear curve is derived from the nonlinear curve by selecting a chord corresponding to rated operation. As such, the two curves are close for flux levels below 0.5 volt-sec.

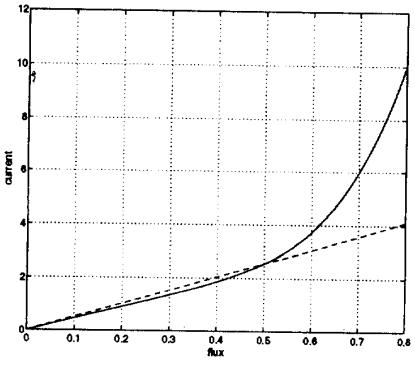

Fig. 6. Stator Flux-Current Characteristics for Saturated and Linear Models

In all experiments, the rotor flux magnitude was programmed in an open-loop manner by simply commanding a constant level of direct axis stator flux. With this simplification, only the stator side flux-current characteristic is needed for use in the rotor flux estimation step. In the stator-based rotor flux observer, the low frequency corner (K_o) was set at 5 rad/sec. For control of the stator flux vector, our system used a bandwidth of 200 rad/sec. This is conservative considering the 15KHz switching frequency and 1KHz update rate.

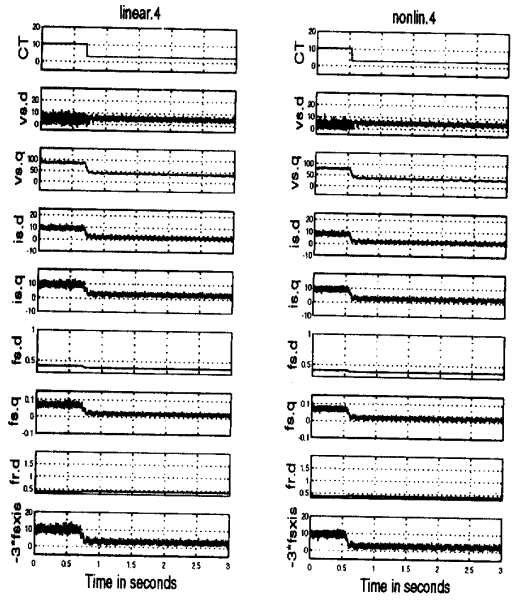

Fig. 7. Comparison of Step Responses with Flux at 0.4 volt-sec. The y-axis labels from top to bottom are CT-Command Torque in N-m, vs.d-direct stator voltage command, vs.q-quadrature stator voltage command, is.d-direct measured stator current, is.q-quadrature measured stator current, fs.d-direct estimated stator flux, fs.q-quadrature estimated stator flux, fr.d-direct estimated rotor flux, -3*fsxis-estimate of actual torque, from the cross product of stator current and stator flux.

Step response data with the commanded rotor flux set at 0.4, 0.5, 0.6, and 0.7 volt-sec were taken. The performance of the control systems based on the linear and nonlinear models are compared in Figures 7-10. These experiments were conducted with a commanded high to low torque step of 10.5 N-m to 1.5 N-m. A computed torque is derived from measured stator current and stator flux via equation (12), shown by the y-axis label $-3f_s \times i_s$. The overall performance of our control system can be evaluated by comparing the computed and commanded torque quantities.

In Figures 7 and 8, the performance with the linear and nonlinear models are not very different. This can be attributed to the fact that the stator is operating unsaturated. However, the step responses with the linear

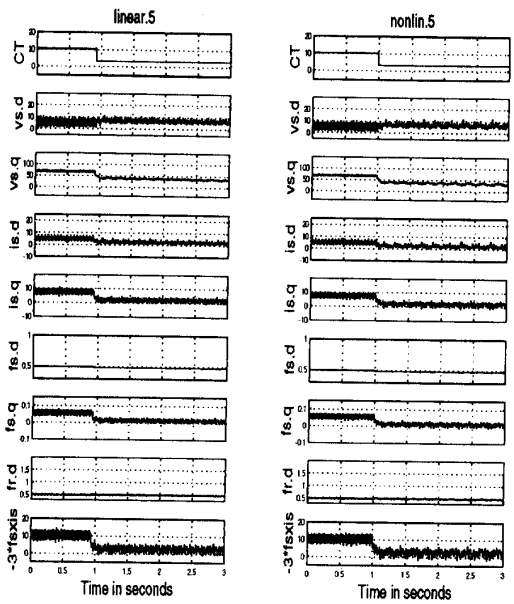

Fig. 8. Comparison of Step Responses with Flux at 0.5 volt-sec. The variables are defined in Figure 7.

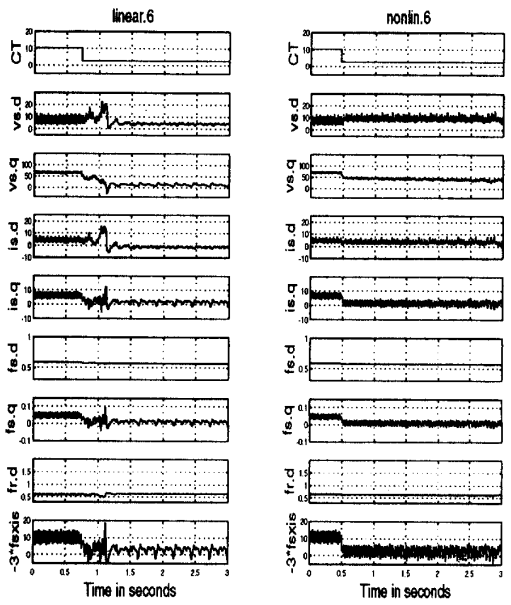

Fig. 9. Comparison of Step Responses with Flux at 0.6 volt-sec. The variables are defined in Figure 7.

and nonlinear models at the higher flux levels (0.6, and 0.7 volt-sec) are drastically different. With the nonlinear flux-current model, our control system generates an essentially ideal transient response to a step torque command, as seen in Figures 9 and 10. In contrast, with the linear flux-current model, calibrated for 0.5 volt-sec, the transients are far from ideal, as seen in these two figures. Specifically, the estimated rotor flux and corresponding computed torque exhibit overshoot and ringing in response to the step command. Note that the rotor flux is estimated using the *linear* magnetic model here. This transient response manifests itself with corresponding behavior on the stator terminals. Namely, the stator current and voltage exhibit similar overshoot and ringing. This behavior corresponds to that exhibited in a detuned field-oriented control scheme, and is due to the neglect of the magnetic saturation.

VII. Conclusion

The new nonlinear π model of induction machine operating in magnetic saturation is more closely based on a physical model of the machine than is the T model. It is also more convenient to use in control design. Methods similar to standard field-oriented control can be developed relatively easily for this model. Flux observers for use with field-oriented control have also been developed. It is expected that these control systems will have higher performance than those based on the T model, both because they are based more closely on the physics of the machine, and because they can be implemented without the approximations that are necessary to derive a reasonably simple control system from the T model.

An experimental implementation of a control system for a 3 hp machine using a voltage-source inverter and a stator-based rotor flux observer was implemented using a commercial inverter and a 386-based computer. The system demonstrated substantial improvements in step response when control based on linear magnetics was replaced with control based on the nonlinear π model.

References

[1] J. E. Brown, K. P. Kovacs, and P. Vas. A method of including the effects of main flux path saturation in the generalized equations of a.c. machines. *IEEE Transactions on Power Apparatus and Systems*, PAS-102(1):96–103, January 1983.

[2] P. Vas, K. E. Hallenious, and J. E. Brown. Cross-saturation in smooth-air-gap electrical machines. *IEEE Transactions on Energy Conversion*, EC-1(1):103–109, March 1986.

[3] Russel J. Kerkman. Steady-state and transient analysis of an induction machine with saturation of the magnetizing branch. *IEEE Transactions on Industry Applications*, IA-21(1):226–234, January/February 1985.

[4] Jean Robert. A simplified method for the study of saturation in a-c machines. In J. Robert and D. K. Tran, editors, *Modelling and Simulation of Electrical Machines and Power Systems*, pages 129–136. Elsevier Science Publishers B. V., North-Holland, 1988.

[5] M. S. Garrido, L. Pierrat, and E. Dejaeger. The matrix analysis of saturated electrical machines. In J. Robert and D. K. Tran, editors, *Modelling and Simulation of Electrical Machines and Power Systems*, pages 137–144. Elsevier Science Publishers B. V., North-Holland, 1988.

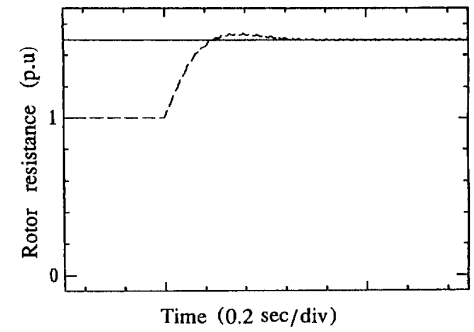

Fig.18 (a) Estimated rotor resistance.

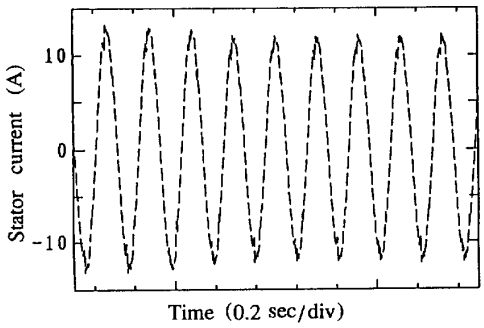

Fig.18 (b) Stator current wave form.

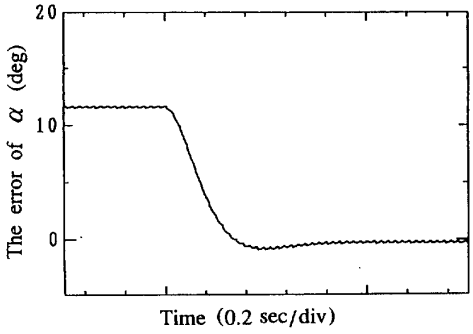

Fig.18 (c) Error of α between the actual and reference.

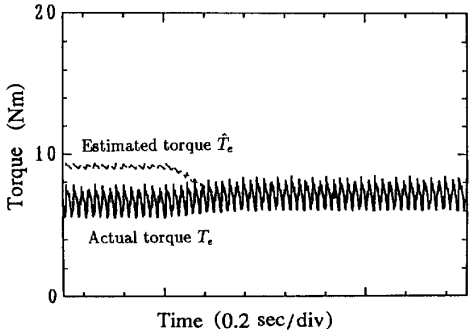

Fig.18 (d) Estimated and actual torque.

Fig.18. Evaluation of Parameter adaptation.

where the rotor speed is 120 r/min at the steady state, the reference magnetizing current i_{mr} is 10 A, the load torque is 6.0 Nm (about 20 % of the rated torque). As the machine nominal parameter, the values given in Table I is used. The rotor resistance of the machine model was increased with step-change 50% more than the nominal value, while the set rotor resistance in the control part is still kept at the nominal value. In this case, the stator current wave form supplied to the motor model is shown by the dashed line in Fig.17(a). For the reference, if there is no change of the rotor resistance, then the current wave form becomes the solid line in Fig.17(a). Fig.17(b) shows the error of α between the actual and the reference. Since α is the angle between $\boldsymbol{i}_s$ and $\boldsymbol{i}_{mr}$, this error causes the error in the estimated torque. It can be understood apparently from (8). Fig.17 (c) shows the estimated torque indicated by the dashed line and the actual one indicated by the solid line, where the deviation of the estimated torque from the actual value is caused by the error of α.

Next the parameter adaptation proposed in Section V was tested in the introduced conditon in Fig.17. Fig.18 (a) shows the estimated rotor resistance by the parameter adaptation and the actual rotor resistance in the machine model, where both of them are indicated by the dashed and the solid line respectively. The estimated rotor resistance converges to the actual value within 0.8 seconds. This convergence time is seems to be sufficiently fast because the real rotor resistance varys slowly due to temperature. In Fig.18 (b), the stator current wave is shown by the dashed line, where it should be noticed that the amplitude is adjusted as the rotor resistance converges. Fig.18 (c) shows the error of α between the actual and the reference, and Fig.18 (d) shows the estimated torque and the actual one. The error of α and the deviation of the estimated torque from the actual value are also corrected as the rotor resistance converges.

These simulation results show the parameter variation effects to the system and the necessity of the parameter adaptation. Next, the experiments are done in the same condition as that of the simulation.

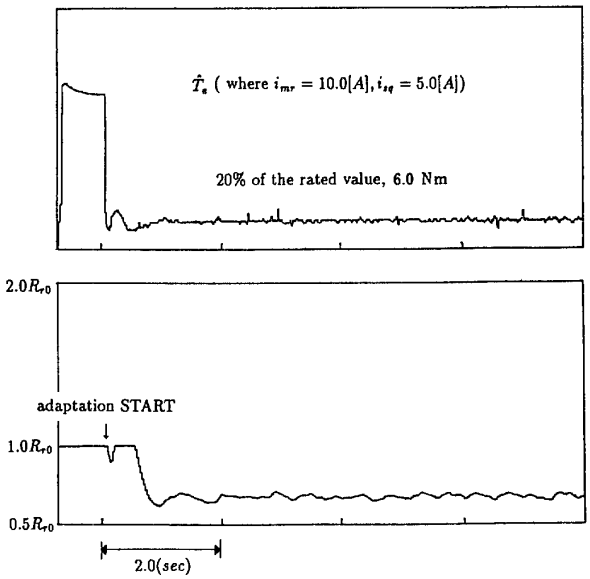

Fig.19. Estimated torque responses and Estimated rotor resistance (i_{mr} = 10 A).